Hindawi
Advances in Civil Engineering
Volume 2020, Article ID 6836492, 20 pages
https://doi.org/10.1155/2020/6836492

Research Article

Study on Construction Influence of Shield Tunnel of Urban Rail Transit on Large-Section Mining Tunnel

Junru Zhang, Lun Ye, Congwen Yan, Bo Yan, Pengru Wei, and Jimeng Feng

Key Laboratory of Transportation Tunnel Engineering, Ministry of Education, Southwest Jiaotong University, Chengdu, Sichuan 610031, China

Correspondence should be addressed to Jimeng Feng; fengjm@swjtu.edu.cn

Received 23 May 2019; Revised 27 December 2019; Accepted 6 January 2020; Published 5 February 2020

Academic Editor: Giosuè Boscato

Due to the increasingly expanding of urban rail transit, shield tunnelling adjacent to existing tunnels has become more and more common in cities. Construction of new tunnels will pose great risks to the safety of existing tunnels. This paper focused on the influence of shield tunnelling on the large-section mining tunnel in the argillaceous siltstone stratum and proposed the influence zone based on the surface subsidence criterion. By carrying out numerical simulations and model test, the surface subsidence, the internal force of the mining tunnel, and the surrounding rock pressure were monitored and the accuracy of the influence zone was verified. The research shows that the shield machine tunnels forward from one time the excavation diameter before the monitoring section until the monitoring section completes the segment assembly. This process is the main stage that causes the increase in the corresponding surface settlement and the additional displacement of the existing mining tunnel. The excavating tunnel influences on the mining tunnel structure were mainly shown at the vertical additional deformation, which is manifested as the overall floating of the mining tunnel. The influence of internal force was performed as the asymmetric change of internal force of the mining tunnel. The mining tunnel is closer to the shield tunnel, showing more significant changes of the internal force of the structures. The structure near the shield tunnel is strengthened by pressure, and the structure far away from the shield tunnel is more prone to tensile failure.

1. Introduction

In recent years with the rapid urbanization in China, the scale of the urban rail transit network has increased sharply. In this case, the construction of tunnels adjacent to existing tunnels becomes more common. Therefore, excavation of the tunnel influences on the existing tunnels to ensure the safety of both tunnels, in terms of the excavation tunnel and the existing tunnel, and surface buildings during the construction are studied [1, 2].

When two or more tunnels are constructed at a close range, the initial stress field of the tunnels will be disturbed. This will lead to the stress change of existing and new tunnel supporting structures. Various problems such as selection of construction methods, procedure, and construction countermeasures have been studied by many researchers [3–6]. Meanwhile, the influence induced by tunnel adjacent construction has been widely discussed. Common research methods nowadays to study this specific issue are theoretical solutions [7–10], numerical simulations [11], and model tests [12].

Many scholars have studied the mechanics behaviour of the adjacent construction of shield tunnels. It has been found that there was a longitudinal effect on the influence of shield construction on existing tunnels, which is manifested by the advance arrival of stress and the lag development of rock mass deformation [13]. Based on the parallel construction of the shield tunnel of the Xi'an Rail Transit Line and CRD tunnel, Kong et al. [14] analysed the surface deformation, intermediate soil stress, and plastic zone of surrounding rock caused by successive construction of the CRD method and the shield method by numerical simulation. Daiguo et al. [15] carried out numerical simulation and field test on the short-distance construction of two shield tunnels and concluded that the short-distance construction of the subsequent tunnel would cause the secondary additional stress

of the first hole segment. Lin et al. [16] investigated the deformation behaviour of the existing tunnels induced by shield tunnelling. The results show that due to oblique intersection, the transverse deformation and internal force of the existing tunnel show obvious asymmetric characteristics. Similarly, Jin et al. [17] analysed the deformation of the existing tunnel and the additional stress caused by shield tunnelling underneath. An empirical formula for the settlement of existing tunnels caused by new shield tunnels was proposed. Qian et al. [18] analysed the settlement characteristics of different intersection angles between high-speed railway and shield tunnel. A safety assessment for the shield tunnel under through high-speed railway was proposed. Meanwhile, the influence zone of shield tunnelling has also been discussed. Ming-nian et al. [19] simulated the full tunnelling process of the shield tunnel. Based on the Mohr–Coulomb yield criterion, the overlapping section of shield tunnels was divided horizontally. Ding et al. [20] studied the influence of new shield tunnels on existing subways and obtained deformation, internal force variation of lining of the existing metro, and its influence zone.

According to the above references, most studies were focused on shield tunnelling under through existing structures and a few papers have focused on shield tunnelling that is adjacent to the large-section mining tunnel. The large-section tunnel was decided to be excavated by steps and parts. When the shield tunnel passes during the excavation, the surrounding rock has already been disturbed many times which induce ground surface settlement. Therefore, the influence zone based on the surface subsidence criterion is proposed in this paper.

Shield tunnelling has become a research hotspot these years. Numerical simulation is the most commonly used method to study this topic [21–23]. Empirical methods and theoretical analyses are used to predict surface settlement and stratum movements caused by shield tunnelling [24, 25]. Model tests also play an important role in investigating mechanical behaviour of shield tunnelling [26–29]. Meanwhile, in order to obtain the real data of shield tunnel, construction field monitoring also has been adopted [30, 31]. Because of the complexity of shield tunnel adjacent construction, using the single method cannot get accurate conclusion. Therefore, numerical simulations and a large scale model test have been adopted in this paper.

Based on the above background, this paper presents a case of the shield tunnelling adjacent to the mining tunnel in Changsha, China. The paper consists of three parts. First, a model test based on the case has been designed. Then, the corresponding numerical simulation has been carried out and the difference of results between the numerical simulation and model test has been discussed. Finally, based on the surface subsidence criterion, the influence zone has been proposed by considering the influence of tunnel clear distance and buried depth.

2. Project Overview

2.1. Engineering Survey. Changsha Metro Line 3 generally is layed at a southwest-northeast direction. In order to meet the future operation needs and be convenient for train stopover and maintenance, the transition line is set up on the right line between the Houjiatang Station and Dongtang Station. The shield construction tunnel and the CRD method construction tunnel were on the left and right, separately. The mileage of the left-line tunnel is from ZDK18 + 515.930 to ZDK19 + 449.825. The mileage of the right-line tunnel is from YDK19 + 226.644 to YDK19 + 449.825. In this case, the minimum clear distance between the two tunnels is noticeably only 4.64 m.

In the field construction, due to the limitation of site size and the construction period, the construction of the right-line mining section was carried out first. The construction of the tunnel was stopped after partial mileage completion, waiting for the left-line shield tunnel to complete the construction. Then, the construction of the right-line mining section was continued until completion. Considering the structural safety of the tunnel by the mining method, the temporary support of the tunnel by the mining method was not dismantled before the shield tunnel passed through. The construction plan of the shield tunnel and mining section is shown Figure 1.

2.2. Engineering Geological Conditions. The interval between the Houjiatang Station and Dongtang Station belongs to the third grade terrace of the Xiangjiang River. The underlying bedrock mainly consists of argillaceous siltstone and conglomerate. The thickness of the overburden layer is between 7.2 m and 19.5 m. The stratum that the tunnels passed through is moderately weathered argillaceous siltstone and conglomerate, partly through strongly weathered argillaceous siltstone. The comprehensive surrounding rock of the tunnel is grade V based on the classification of the rock mass. The layout of tunnel cross section is shown in Figure 2, and the physical and mechanical parameters of each soil layer are shown in Table 1.

Based on the geological survey data, the stratum which the tunnel passes through is mainly argillaceous siltstone stratum. The average thickness of other overburden layers is smaller than the depth of the mining tunnel. Moreover, the distribution of the overlying strata is complex. Therefore, both numerical simulations and the model test are only simulated for argillaceous siltstone formation.

2.3. Design and Construction Scheme. The shield method has been adopted in the left-line section. The shield excavation diameter is 6.28 m. C50 concrete single-layer assembled segment lining has been chosen. The thickness of segments is 0.3 m, and the width is 1.5 m. The inner and outer diameter of the tunnel is 5.4 m and 6 m, respectively. On the contrary, the CRD method has been used in the right-line. The maximum width is 14 m, and the maximum height is 11.37 m. The maximum excavation area of the design section is 130.2 m^2. A grille steel frame has been set every 0.5 m, and the C25 shotcrete with a thickness of 30 cm has been applied. I-beam frame and C25 shotcrete with a thickness of 25 cm have been used in the middle wall and temporary inverted arch.

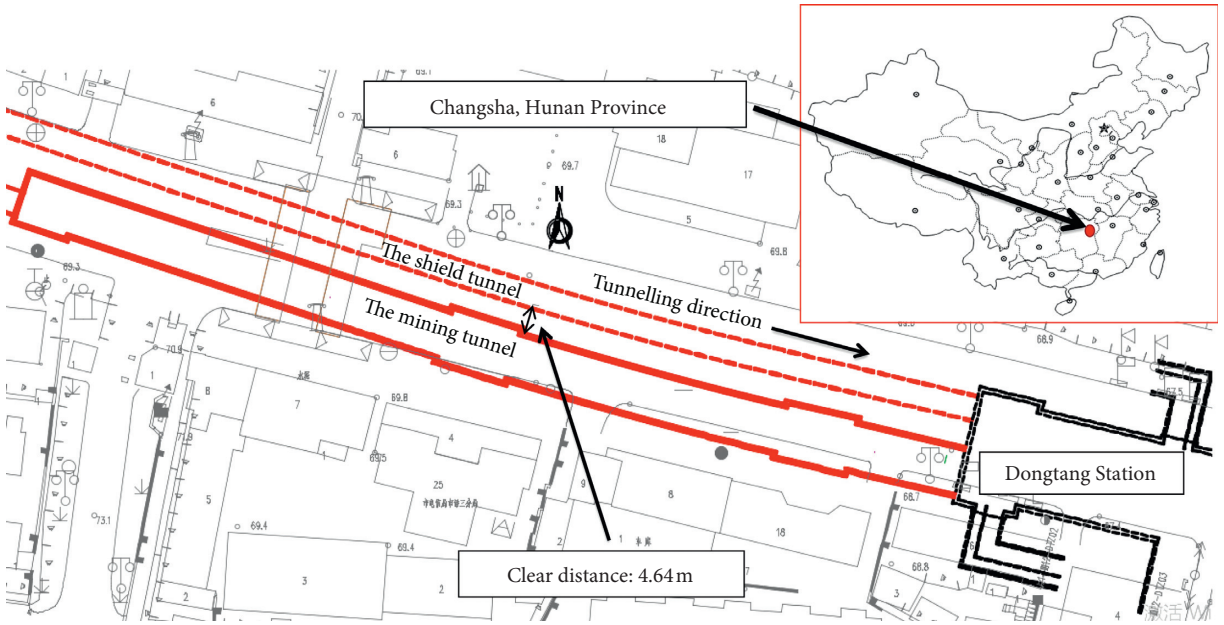

Figure 1: The layout of the construction plan (unit: m).

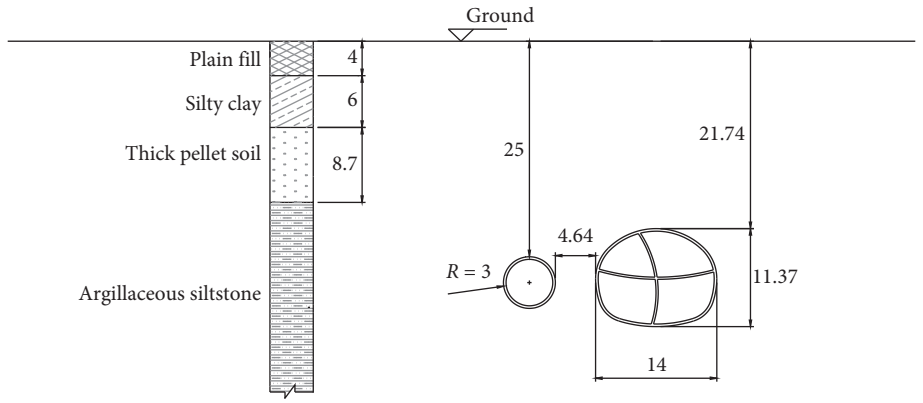

Figure 2: Schematic diagram of the cross-section arrangement of tunnels (unit: m).

Table 1: Stratigraphic physical and mechanical parameters.

Sequence	Soil layer	Elastic modulus (MPa)	Cohesion (kPa)	Poisson's ratio	Internal friction angle (°)	Unit weight (kN/m^3)
1-2-2	Plain fill	2.6	10	0.30	12	18.5
3-1	Silty clay	20.4	23	0.31	15.4	19.1
3-8	Thick pellet soil	46.8	0	0.22	36	18.6
7-2-3	Argillaceous siltstone	700	100	0.35	23.5	24.1

3. Model Test of Engineering Example

In order to study the influence of the shield tunnel on the construction of the existing tunnel, this paper simulates the construction process of the shield excavation by the model test. Surface subsidence, changes in surrounding rock stress, and internal forces of the mining tunnel model were monitored.

3.1. Similarity Ratio Determination. Considering the feasibility of simulated shield excavation, the limitation of the size, and bearing capacity of the model test equipment, the similarity ratio of the weight C_γ and the geometrical similarity C_l is 1 and 20, respectively. Based on the similarity theory, the similarity ratios of various parameters are obtained. The similarity ratio of strain, Poisson's ratio, and internal friction angle satisfies $C_\varepsilon = C_\mu = C_\varphi = 1$. Moreover, the similarity ratio of stress, cohesion, and elastic modulus satisfies $C_\sigma = C_c = C_E = 20$. The model geometry and arrangement position are shown in Figure 3.

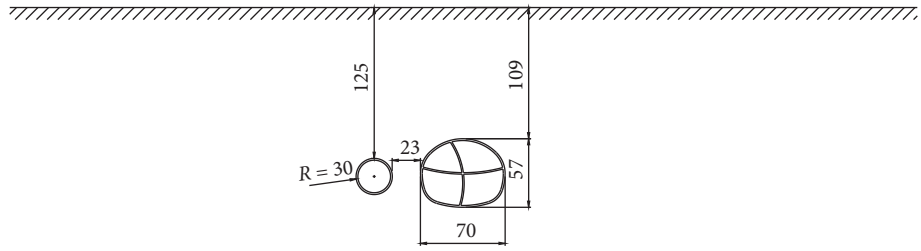

Figure 3: Model placement relative position and geometry (unit: cm).

3.2. Preparation for Model Test

3.2.1. Model Test Box. The size of the model box is 3 m × 3 m × 1 m. The model test box was made of welded steel plate, and the steel plate surface of the box was provided with ribs at a certain interval to ensure that the lateral deformation of the model box will not affect the test results. On the one hand, the acrylic plate which has been used in the model test, as shown in Figure 4, can meet the requirements of strength and deformation. On the other hand, it is convenient to observe the model failure during the test. Therefore, the opening of the model box is connected with the steel plate by the acrylic plate, as shown in Figure 4.

3.2.2. Similar Materials for Surrounding Rock. Unit weight, elastic modulus, Poisson's ratio, internal friction angle, and cohesion are the significant configuration control parameters of surrounding rock materials. They should meet the requirements of the changing ratio, easily adjusting the physical and mechanical properties. Moreover, they should be less interfered by the external environment. According to references [32, 33], the mixture of river sand, quartz sand, barite powder, fly ash, and engine oil has been selected as the surrounding rock simulation material. Barite powder can effectively increase the bulk density. Quartz sand can increase the friction angle, and engine oil can change the internal friction angle.

Base on the similarity ratio, the mechanical parameters of similar materials for surrounding rock should be similar to those listed in Table 2.

In order to determine the materials mix ratio, the direct shear test has been conducted. The shear strength of similar materials can be established by the direct shear test. The principle of the direct shear test is to put the sample into a cylindrical shear box. By applying a fixed vertical load on the upper part of the sample and a horizontal displacement with a fixed speed in the horizontal direction, the horizontal shear stress is measured. Then, the normal stress and shear stress on the shear plane can be calculated. The shear strength envelope also can be determined after the normal stress, and shear stress values of several groups of samples are obtained. The direct shear apparatus and failure of the test after the direct shear test are shown in Figure 5.

After the direct shear test, calculate the shear stress of the sample according to the following equation:

$$\tau = \frac{CR}{A_0} \times 10, \tag{1}$$

where τ is the shear stress (unit: kPa); C is the calibration coefficient (unit: N/0.01 mm); R is the dynamometer reading (unit: 0.01 mm); A_0 is the section area of the sample (unit: cm^2); and 10 is the unit conversion factor.

By carrying out direct shear tests under multiple sets of mixing ratios, the mix ratio of surrounding rock materials is obtained, as shown in Table 3. The direct shear test results of similar materials with this mix ratio are shown in Table 4. It can be found that the mechanical parameters of similar materials at this mixing ratio are similar to the theoretical value.

3.2.3. Similar Materials for Supporting Structure. The shield segment, initial support, and temporary support of the mining tunnel simulated in this test were all made of acrylic. Acrylic material is uniform, easy to process, and has good durability. It can be used as a similar material for the supporting structure. Therefore, based on the principle of the model similarity ratio and equivalent bending stiffness, the dimensions of similar models are calculated as shown in Table 5.

Therefore, the shield tunnel segments, initial support, and temporary support were made by acrylic sheets of 10 mm, 12 mm, and 10 mm thick, respectively, as shown in Figure 6.

3.2.4. Excavation Simulation of Shield Tunnelling Method. In order to simulate the shield tunnelling process, a shield tunnelling simulation machine is designed. The composition of the shield construction simulator is shown in Figure 7.

The simulation process is as follows:

Position the simulated machine.

According to the required pushing pressure, put the corresponding weight of the weights on the plate and push the sliding car through the fixed pulley.

Rotate the main shaft of the steel pipe to drive the cutter head to rotate and cut the soil in front.

With the mechanical excavation, the acrylic tube model is pushed in and the muck in the shield model is extracted with a tool.

(a) (b)

Figure 4: Model test box.

Table 2: Theoretical value of mechanical parameters of similar materials for the surrounding rock.

Project	Unit weight (kN/m^3)	Elastic modulus (GPa)	Poisson's ratio	Cohesion (kPa)	Internal friction angle (°)
Prototype	24.1	700	0.35	100	23.5
Model	24.1	35	0.35	5.3	23.5

(a) (b)

Figure 5: Direct shear test. (a) Direct shear apparatus; (b) failure surface of the direct shear test.

Table 3: Model of surrounding rock with similar material mix ratio.

Material	Proportion
Barite	1
Fly ash	1
River sand	0.5
Coarse quartz sand	0.25
Fine quartz sand	0.5
Engine oil	0.32

Record the length of the mechanical excavation according to the scale on the sliding rail and record the time.

During the simulation, keep the cutter head rotating at a constant speed. Remove the slag in time to avoid affecting the cutter head. The shield segment model should be close to the cutter head to avoid excessive gaps.

3.3. Model Test Procedures

3.3.1. Test Component Installation. In the process of the simulation, surface subsidence, surrounding rock pressure, and structural stress of the mining method were monitored. The monitoring section was arranged at 25 cm along the

Table 4: Results of the direct shear test.

Vertical stress (kPa)	Shear stress (kPa)	Displacement (0.01 mm)	Fitting equation	Internal friction angle (°)	Cohesion (kPa)
100	53.3216	30.4	$y = 0.4507x + 5.3372$	24.26	5.3372
150	72.2648	41.2			
200	90.6818	51.7			
300	143.1264	81.6			

Table 5: Thickness of acrylic models.

Project	Shield tunnel segment (C50)		Initial support (C25)		Temporary support (C25)	
	Elastic modulus (GPa)	Thickness (mm)	Elastic modulus (GPa)	Thickness (mm)	Elastic modulus (GPa)	Thickness (mm)
Prototype	34.5	300	28	300	28	250
Model	2.86	12.68	2.86	11.83	2.86	9.85

Considering the joint effect of the shield segment, the equivalent stiffness is reduced to 80% of the C50 reinforced concrete and the thickness of the similar material is about 10 mm.

(a) (b)

Figure 6: Acrylic tunnel model. (a) Model of the mining tunnel; (b) model of the shield tunnel.

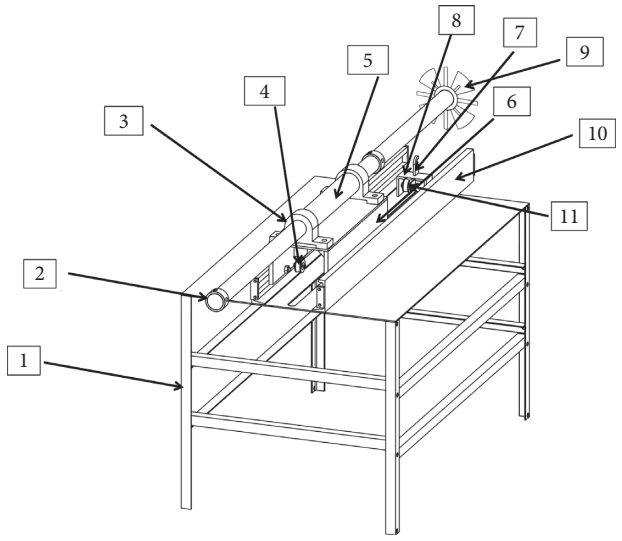

Figure 7: Shield construction simulation machinery. 1, test bench; 2, rotating shaft socket; 3, bearing block; 4, fixed pulley 1; 5, steel tube shaft; 6, sliding car; 7, hook; 8, pulley bracket; 9, replaceable cutter head; 10, sliding rail; 11, fixed pulley 2.

direction of shield tunnelling. The position of the internal force monitoring point is shown in Figure 8.

A strain gauge has been attached to the inner and outer sides of each measuring point in the initial support. An earth pressure box is set along the outer surface. A strain gauge is attached to the inner and outer sides of each measuring point in the temporary support, and four earth pressure boxes are set around the shield tunnel. After the strain gauge has been affixed, cover it with silica gel to ensure the connection was firm, subsequently checking the connection at each point was working. The actual arrangement of measurement points is shown in Figure 9.

Before the shield was excavated, the earth pressure boxes around the shield tunnel were buried in the designated location in the model test. At the same time, the mining tunnel model has been put into the design position, using a ground displacement gauge with an accuracy of 0.01 mm, and four measuring points are arranged according to Figure 10 on the corresponding surface of the monitoring section. The initial reading is recorded. The actual arrangement is shown in Figure 11.

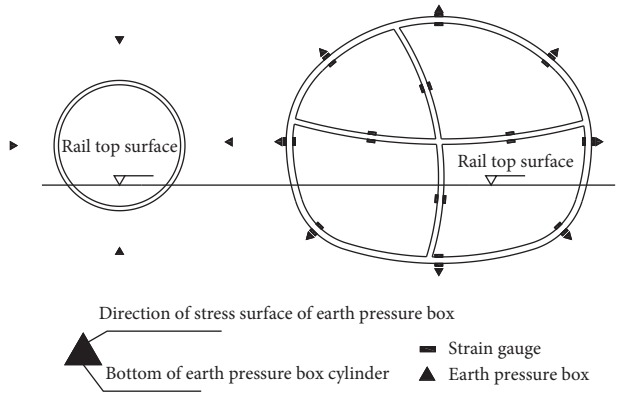

Figure 8: Monitoring section and monitoring point arrangement.

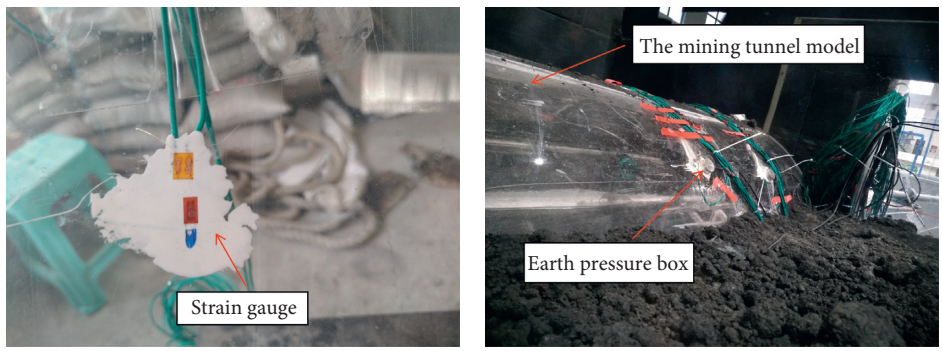

(a) (b)

Figure 9: Strain gauge and earth pressure box arrangement.

3.3.2. Shield Simulation Machinery Installation. Rotate the main shaft of the steel pipe to drive the cutter head to rotate and cut the soil in front, as shown in Figure 12. Later, the acrylic shell model has been pushed in to simulate the segment assembly after the shield machine passes though the soil. Collect the testing data of test components on the monitoring section as the excavation progresses.

3.4. Test Results

3.4.1. Analysis of Earth Pressure around the Tunnel. The earth pressure values at each measuring point were obtained through monitoring. The relationship between shield tunnelling distance and test time is shown in Figure 13. The curves of earth pressure changes at each measuring point are shown in Figures 14 and 15. If the changing of the earth pressure relative to the initial stress is positive, it indicates that the earth pressure at the measuring point decreases. Otherwise, it indicates that the earth pressure increases.

The changing value of soil stress at each measuring point of shield tunnelling is shown in Table 6. Due to the preheating of the test instrument 40 minutes in advance, the initial changing of earth pressure is basically zero. There were four stages in the change of earth pressure around the shield tunnel: sharp change ⟶ slow change ⟶ sharp change ⟶ relatively stable. When the shield tunnel was excavated at the distance of 25 cm, the maximum pressure change of the upper part of the shield was 8.41 kPa. The change of earth pressure on the left, under, and right sides of the shield was 3.30 kPa, 6.07 kPa, and 6.38 kPa, respectively. The left wall of the mining tunnel was in the position with the minimum horizontal distance between the two tunnels. The changing of surrounding rock pressure was 4.53 kPa. It reveals that the shield excavation has made the initial surrounding rock stress at these positions to be released gradually. However, the variation of earth pressure at other measuring points was very small. When the shield tunnel was excavated at the distance of 30 cm, the measured pressure changes at the left and right side of the shield tunnel and the left wall of mining tunnel were noticeably changed, reaching at 6.89 kPa, 8.37 kPa, and 7.57 kPa, respectively. When the shield tunnel was excavated at the distance of 35 cm, except a small amount of decrease in the change of earth pressure at the left wall of the mining tunnel, the earth pressure at other positions has relatively not changed. Based on the 174-minute to the end of the 230-minute recording, the earth pressure value of each position showed almost no change, which indicate that the stress field of the surrounding rock no longer changes.

It can be found from the analysis of the variation law of the surrounding rock stress in the process of shield construction that the construction of the shield tunnel will cause

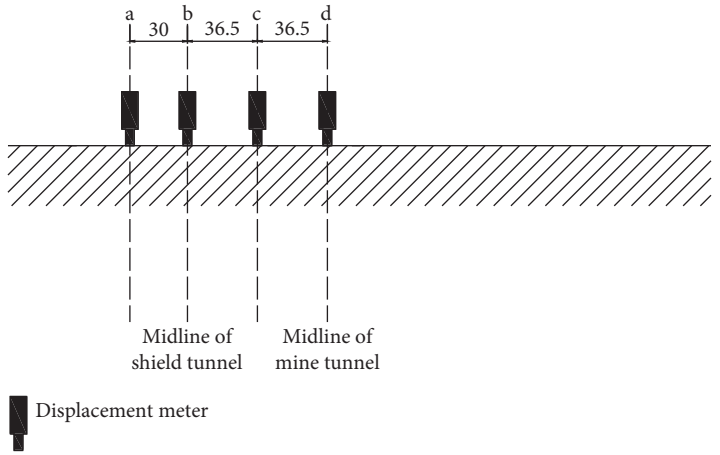

Figure 10: Layout of monitoring points for surface subsidence (unit: cm).

(a) (b)

Figure 11: Ground displacement meter and arrangement. (a) Ground displacement meter; (b) arrangement of ground displacement meter.

(a) (b)

Figure 12: Shield tunnelling simulation.

the changing of surrounding rock stress around the existing tunnel. There are different distribution rules of stress changes in different positions of initial support induced by shield tunnelling. The changing of the rock stresses was more severe as it was more closer to the shield tunnel.

3.4.2. Internal Force Analysis of Tunnel by Mining Method. The test results were the strain values of each measuring point. According to $\sigma = E\varepsilon$, the inner and outer stress values σ_{in} and σ_{out} can be obtained. Then, the axial force N and the bending moment value M of each measuring point are obtained by the following equation:

$$N = \frac{1}{2}(\sigma_{in} + \sigma_{out})b,$$
$$M = \frac{1}{12}(\sigma_{in} - \sigma_{out})bh^2, \quad (2)$$

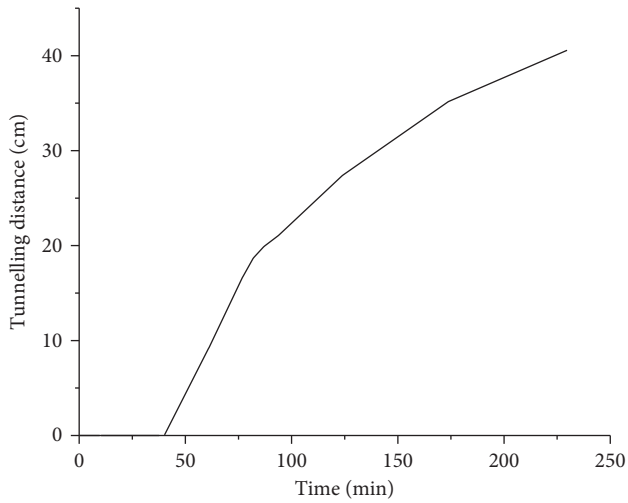

Figure 13: The relationship between shield tunnelling distance and test time.

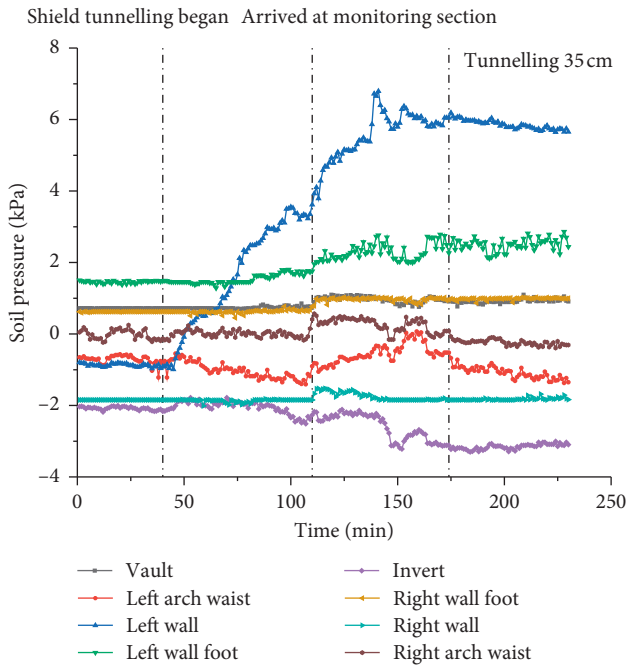

Figure 14: Time-history curve of earth pressure around the mining tunnel.

where b is the thickness of the lining of the mining method model and h is the unit width of lining in the mining tunnel model. The internal forces of initial support and temporary support are shown in Figures 16 and 17.

During the preheating period, the data of each point fluctuate. With the shield tunnelling, the bending moment and axial force of each measuring point have changed obviously. It can be considered that the strain gauges work normally. From Figures 16(a) and 17(a), it can be seen that with the shield tunnelling to the monitoring section, the axial force of the left side structure of the mining tunnel tends to increase. The axial force of the left wall and left wall

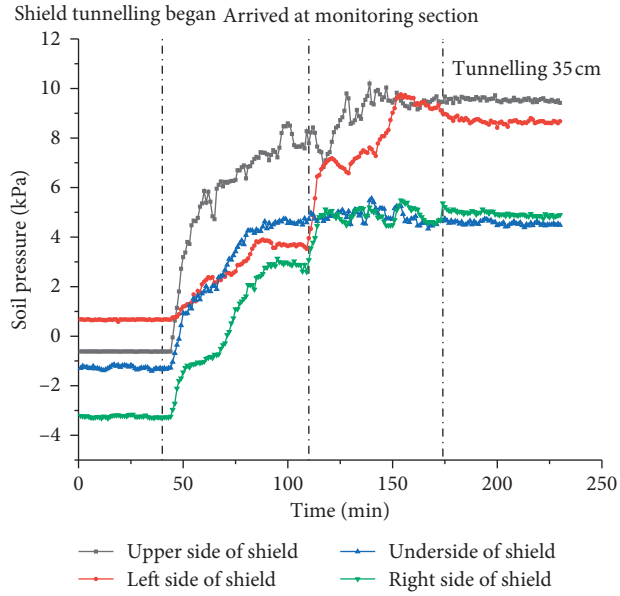

Figure 15: Time-history curve of earth pressure around the shield tunnel.

foot increased by 13.6 N and 11.1 N, respectively. Meanwhile, the axial force of the right-side structure of the tunnel tends to decrease, with the changing of the foot of the right-side wall decreased by 18.4 N. Furthermore, the temporary support axial force decreases obviously with the shield tunnelling.

It can be seen from Figures 16(b) and 17(b), with the shield tunnel passing through the monitoring section, the right wall foot, right wall, and upper part of the middle wall changed significantly and the bending moment at each point has increased by 0.86 N·m, 1.36 N·m, and 1.29 N·m, respectively. Meanwhile, the bending moments at other locations except the left foot of the wall also have increased. The influence of shield tunnelling on the vault and inverted arch was less showing; meanwhile, the increasing rate of the bending moments at the left and right sides of the wall has increased obviously. For the temporary supporting structure, the bending moments at the upper and middle walls have increased noticeably, while the bending moments at other locations were slightly changed. During the test, the maximum compressive stress increment of the left structure was 0.052 MPa and the maximum tensile stress increment of the right structure was 0.056 MPa.

Generally speaking, the left structure was affected by shield tunnelling more severe and the increase of bending moment and axial force was relatively great. When the axial force of the right-side structure decreased and the moment increased, the eccentricity of the right-side structure became larger, which was more prone to tensile failure. The above analysis shows that the excavation of the left shield will cause uneven changes in the internal force of the lining structure of the right-line mining tunnel. The structure near the shield tunnel will be strengthened by compression, and the structure far from the shield tunnel will be more prone to tensile failure.

Table 6: Variation of earth pressure at different measuring points (unit: kPa).

Tunnelling distance	Vault	Right wall foot	Right wall	Right wall waist	Invert	Left wall waist	Left wall	Left wall foot	Upper side of shield	Left side of shield	Under side of shield	Right side of shield
20 cm	0.10	0.04	0.00	0.13	0.13	−0.44	3.59	0.15	8.05	3.19	5.58	5.73
25 cm	0.02	0.15	0.00	0.54	−0.10	−0.09	4.53	0.27	8.41	3.30	6.07	6.38
30 cm	0.25	0.36	0.06	0.40	−0.06	0.49	7.57	1.24	10.03	6.89	6.90	8.37
35 cm	0.19	0.34	0.00	0.21	−0.95	0.30	6.96	0.78	10.08	8.33	6.00	8.67
40 cm	0.21	0.36	0.04	−0.18	−0.87	−0.42	6.66	1.21	10.13	7.94	5.88	8.18

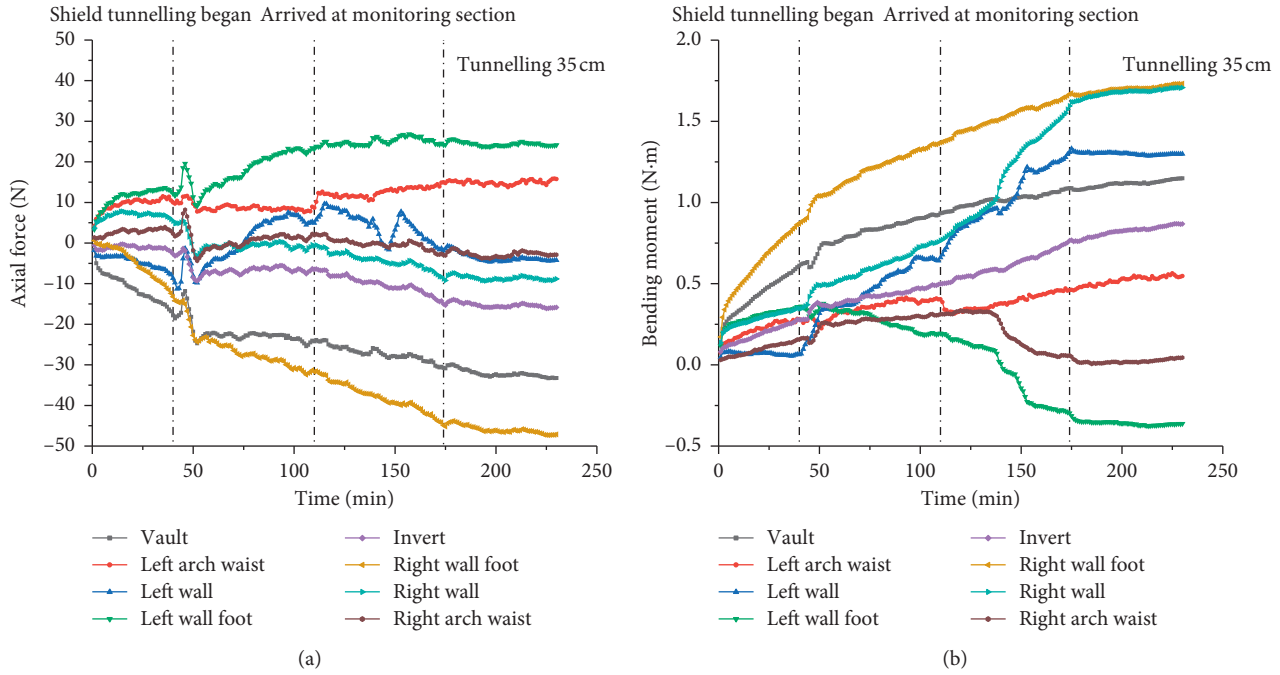

Figure 16: Time-history curve of internal force in initial support. (a) Axial force curve of initial support; (b) bending moment curve of initial support.

3.4.3. Analysis of Surface Settlement. The surface subsidence curve obtained from the test is shown in Figure 18.

According to the foregoing, after 35 cm of shield tunnelling, the surrounding rock pressure of the tunnel and the internal force of the tunnel structure by the mining method basically tend to be stable. So, it can also be considered that the surface settlement tends to be stable. From Figure 18, it can be seen that the maximum value of ground settlement appears on the surface corresponding to the shield tunnel vault and the final settlement value is 0.14 mm. The final settlement of point b is 0.05 mm, and the maximum settlement increment of actual project is 1 mm based on the conversion of the similarity ratio.

4. Numerical Simulation Based on Model Test Prototype

The numerical simulation was based on the construction of the tunnel between the Houjiatang station and Dongtang station of Changsha Rail Transit Line 3. The finite difference software FLAC^{3D} is used for calculation. The relative positions of the two tunnels are shown in Figure 2.

4.1. Numerical Model. The 3D calculation model was established to study the influence of shield tunnelling adjacent to the large-section mining tunnel, as shown in Figure 19. The dimensions of the numerical model are 150 m in length, 70 m in width, and 88 m in height. The model consists of 602634 grid points and 585340 zones. As for the boundary conditions of the model, the displacement of the normal direction of each face of the model was constrained except the top surface.

In numerical simulation, the Mohr–Coulomb elastic-plastic constitutive model was used for the soil layer. Cable element is used for the system-anchoring bolt and advance pipe shed. Elastic solid element was used for segments, initial support, and temporary support of the mining tunnel. Shell element was used for steel shell of the shield machine. The grouting situation and scope of the shield tail gap were very complex. Hence, they are equivalent to elastic, equal

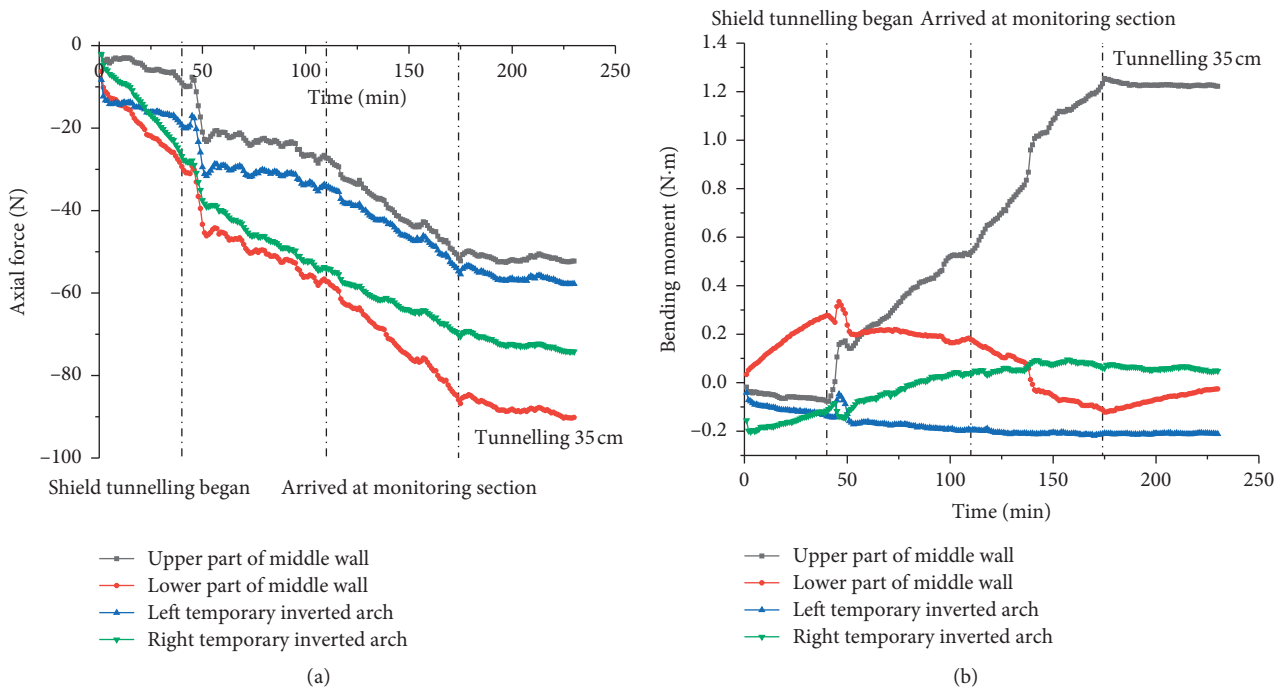

Figure 17: Time-history curve of internal force in temporary support. (a) Axial force curve of temporary support; (b) bending moment curve of temporary support.

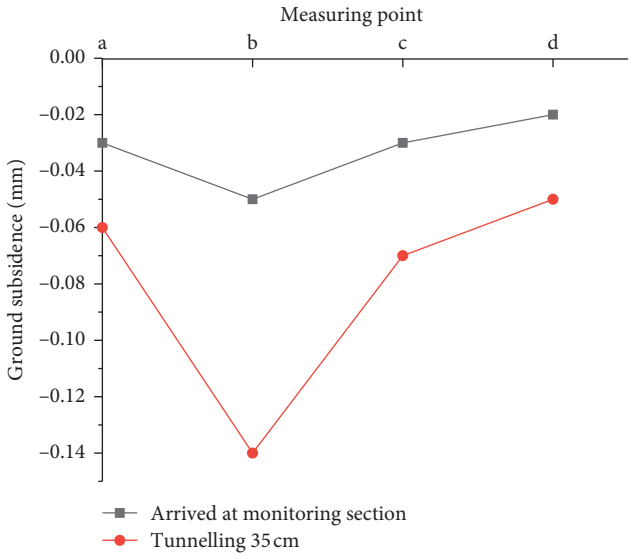

Figure 18: Surface settlement curve.

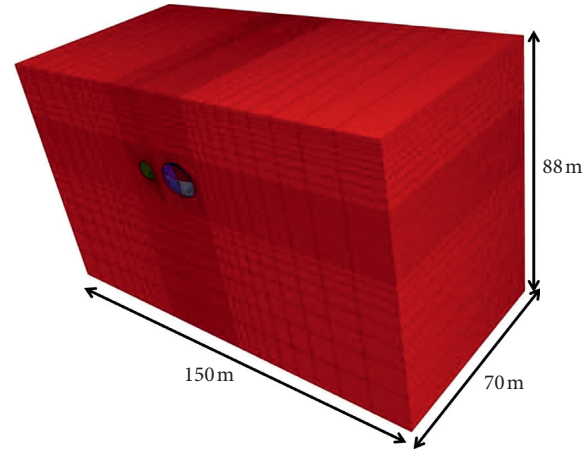

Figure 19: Numerical calculation model.

thickness, and uniform equivalent layer [34–36], which was modeled as the elastic solid element with a thickness of 14 cm. The numerical calculation parameters of various structures are shown in Table 7.

4.2. Tunnel Construction Simulation

4.2.1. Simulation of Mining Tunnel. As shown in Figure 20, the mining tunnel is excavated in the order of 1#-3#-2#-4#. The simulated excavation consists of 173 steps with an excavation length of 0.5 m for each step. When the construction of the mining tunnel has been completed, the shield tunnel simulation was started. The temporary support was not dismantled during the whole simulation process.

4.2.2. Simulation of Shield Tunnel. The numerical simulation process of shield tunnelling can be divided into four stages including excavation, grouting at shield tail, detachment of shield tail, and segment bearing. In the numerical calculation, the shell length of the shield machine is 9 m. The simulated excavation consists of 53 steps with an excavation length of 1.5 m which is the width of the segment for each step. The stiffness reduction coefficient of segments is 0.8. The specific numerical simulation process is as follows:

Table 7: Physical and mechanical parameters.

Parameter types	Constitutive model	Elastic modulus (GPa)	Cohesion (kPa)	Internal friction angle (°)	Poisson's ratio	Unit weight (kN/m^3)
Soil layer	MC	0.7	100	23.5	0.35	24.1
Initial support	Elastic	30.5	——	——	0.25	26.4
Temporary support	Elastic	34.7	——	——	0.25	27.1
System anchoring bolt	Elastic-plastic	206	150	24	——	79
Advance pipe shed	Elastic-plastic	206	170	30	——	79
Shield segment	Elastic	37.5	——	——	0.2	26.5
Steel shell	Elastic	206	——	——	0.2	79
Equivalent circle zone	Elastic	1.0	——	——	0.2	20.5

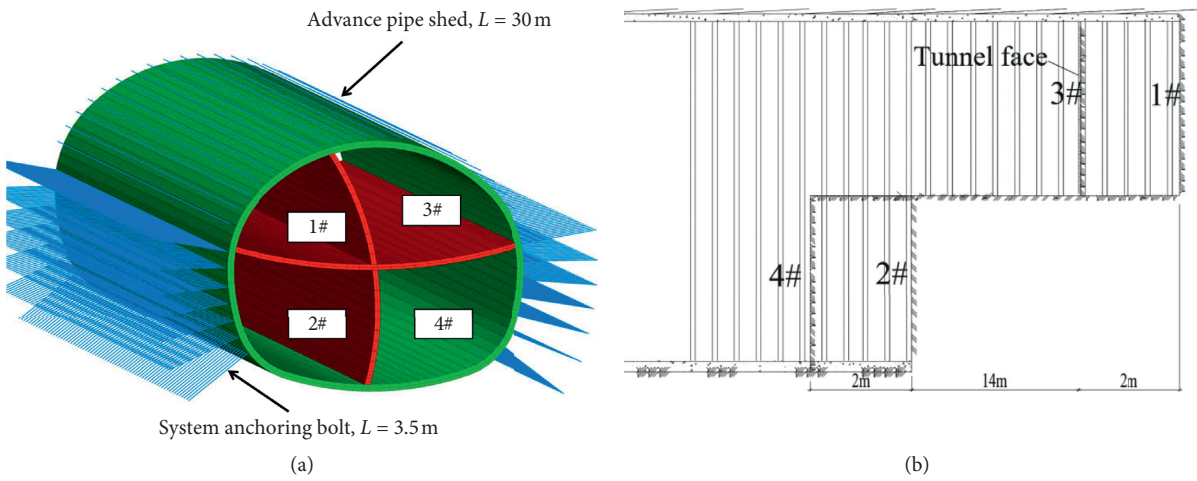

Figure 20: Mining method branch excavation simulation. (a) Mining tunnel excavation model; (b) sequence chart of longitudinal section of the mining tunnel.

(1) Excavation: each tunnelling distance is 1.5 m. Apply 0.25 MPa jacking force on the excavation surface. Meanwhile, activate the shell element to simulate the steel shield of the shield machine.

(2) Grouting at shield tail: delete the shell element of the last ring at the tail of the shield and apply 0.25 MPa grouting pressure on the surrounding rock of the last ring.

(3) Detachment of shield tail: delete the grouting pressure of the second ring behind the shield tail to simulate the state when the segment is separated from the shield tail.

(4) Segments bearing: activate the segments and equivalent layer.

Numerical simulation of shield tunnelling is shown in Figure 21.

4.3. Numerical Simulation Results. The longitudinal section of the numerical model at 35 m is taken as the monitoring section. The surface settlement induced by shield tunnelling, the structural deformation, and the structural stress of the mining tunnel was monitored.

4.3.1. Analysis of Ground Settlement. Figure 22 shows the ground settlement induced by the shield tunnel. The surface settlement corresponding to the vault of shield tunnel (Settlement 1) and the maximum surface settlement (Settlement 2) are shown in Figure 23. In Figure 22, Stage 1 indicates the completion of the construction of the mining tunnel; Stage 2 indicates that the excavation surface of the shield tunnel is 6 m away from the monitoring section; Stage 3 indicates that the shield tunnelling reaches the monitoring section; Stage 4 indicates the completion of the support of the monitoring section; Stage 5 indicates the completion of the construction of the shield tunnel.

After the construction of the mining tunnel, the surface settlement curve is symmetrical along the middle line of the mining tunnel, with the maximum value of 14.6 mm. After the construction of the shield tunnel, Settlement 1 has increased by 1.6 mm, accounting for only 55% of Settlement 1 at Stage 1. Settlement 2 has increased by 0.6 mm, accounting for 3.9% of Settlement 2 at Stage 5. It can be seen that the influence of shield tunnelling on surface settlement was not dominant.

When the left-line shield tunnelling was 6 m (1x diameter) away from the monitoring section, Settlement 1 has changed slightly. Between Stage 1 and Stage 2, Settlement 1

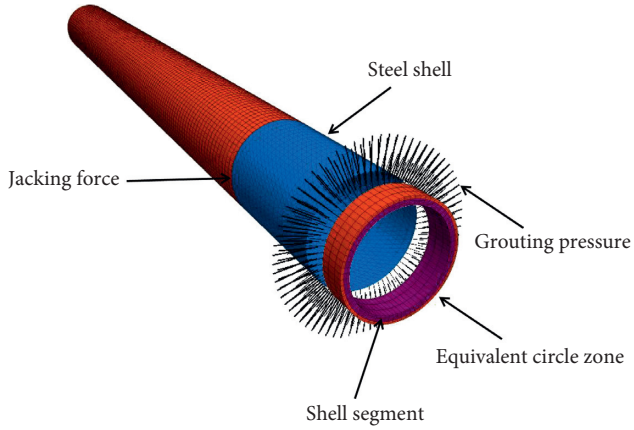

Figure 21: Shield tunnelling simulation.

has increased by 0.1 mm only accounting for 6.3% of the total increment and Settlement 2 also has increased by 0.1 mm accounting for 16.7% of the total increment. After reaching the monitoring section (Stage 3), Settlement 1 has increased rapidly. Between Stage 2 and Stage 4, Settlement 1 has increased by 1.2 mm, accounting for 75% of the total increment. Meanwhile, Settlement 2 has increased by 0.4 mm, accounting for 66.7% of the total increment. The above analysis shows that the shield method is more effective than the mining method in controlling surface settlement. The shield machine tunnels forward from one time the excavation diameter before the monitoring section until the monitoring section completes the segment assembly. This process is the main stage that causes the surface settlement.

4.3.2. Structural Deformation Analysis. As shown in Figures 24 and 25, the change of the additional displacement in the horizontal and vertical directions has been recorded. The horizontal and vertical additional displacements of different measuring points are shown in Table 8.

As shown in Table 8, the influence of the shield tunnelling on the structure of the mining tunnel was mainly a vertical additional deformation. The influence of the left-side structure which was near the shield tunnel was much larger. The mining tunnel has an overall upward trend.

As shown in Figure 24, before Stage 2, the horizontal additional displacement of the mining tunnel has changed slowly. The horizontal additional displacements at Stage 2 of the vault, left wall, invert, and right wall have, respectively, reached 0.05 mm, 0.05 mm, 0.02 mm, and 0.06 mm. After Stage 4, the displacement of each measuring point is basically unchanged. It can be concluded that the influence distance of shield tunnelling on the horizontal additional deformation of the front mining tunnel structure is one times the diameter of the shield tunnel. The horizontal additional displacement of the left wall is most affected by the shield tunnelling. The displacement of the left wall increases much more than that of the other measuring points. The maximum additional deformation of the left wall is 0.42 mm due to the extrusion effect of shield tunnelling.

As shown in Figure 25, at Stage 2, the vertical additional displacements of these measuring points reach 0.06 mm, 0.06 mm, 0.05 mm, and 0.05 mm, respectively, which was only accounting for 28.5%, 26%, 22.7%, and 25.5% of the final variation. At Stage 4, the displacements of these measuring points reach 0.15 mm, 0.18 mm, 0.14 mm, and 0.12 mm, respectively, which was accounting for 71%, 79%, 63.6%, and 61.2% of the final variation. Therefore, it can be concluded that the influence distance of shield tunnelling on the additional deformation of the front mining tunnel structure is one times the diameter of the shield tunnel.

The above analysis illustrates that the shield tunnels forward from one time the excavation diameter before the monitoring section, until the monitoring section completes the segments assembly. This process is the main stage that causes the additional deformation of the mining tunnel structure.

4.3.3. Structural Force Analysis. Figure 26 illustrates the additional internal forces of the tunnel structure induced by shield tunnelling. In Figure 26(a), the right-line mining tunnel was affected by the construction of the left-line shield tunnel. Except the left wall side, foot, and invert, the bending moments of all the other monitoring points have shown no changes. The bending moments of the left wall foot and invert increased by 3.79 kN·m and 0.49 kN·m. In addition, the bending moments of the left wall side decreased by 2.65 kN·m. As Figure 26(b) illustrates, the additional axial forces of the left arch waist, the left wall, and the left wall foot increased by 126.9 kN, 174.6 kN, and 137.2 kN, respectively. However, the axial force of the right structure including the right arch waist, right wall, and right wall foot decreased by −17.8 kN, −33.3 kN, and −10.5 kN, respectively. It can be concluded that compared with the right structure, the left structure is greatly affected by shield tunnelling.

The maximum compressive stress increment of the left structure is 0.71 MPa. The maximum tensile stress increment of the right structure is 0.15 MPa. The reason in this case is because the shield tunnelling disturbed the surrounding rock, which leads to the unloading effect on the surrounding rock of the left side of the mining tunnel. Stress redistribution of the surrounding rock leads to uneven changes in the internal force of the tunnel structure. The structure near

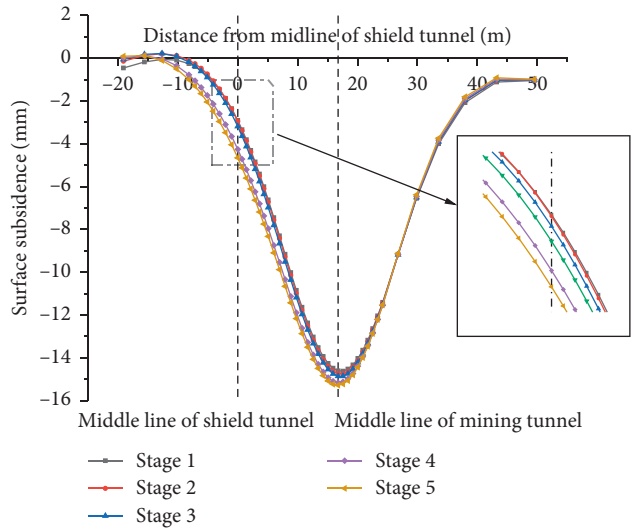

Figure 22: Ground settlement curve after shield tunnelling.

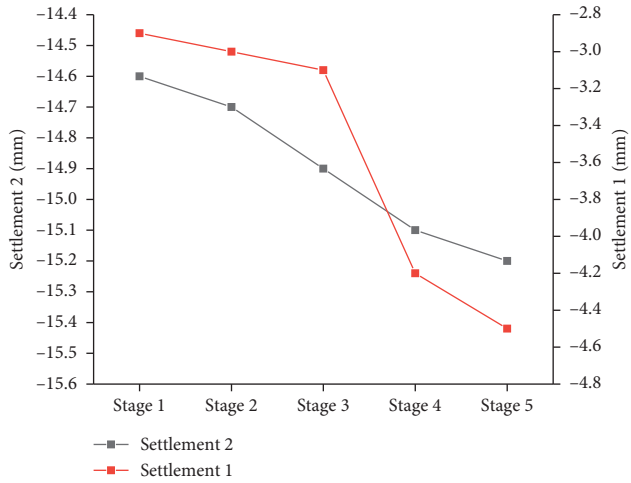

Figure 23: Surface settlement results.

the shield tunnel was strengthened by pressure, and the structure far away from the shield tunnel is more likely to be damaged by tension. The above analysis illustrates that shield tunnelling will cause uneven changes in the internal force of the existing tunnel structure. The structure near the shield tunnel is more affected.

4.4. Comparison of Numerical Simulation and Model Test Results. The results of numerical simulation and model test show that the influence of left-line shield tunnelling on the right-line tunnel structure was manifested by the uneven changes of the internal force in the mining tunnel structure. The closer to the shield tunnel, the more severe the internal force of the structure changes. The model test is consistent with the law obtained by numerical simulation. In the numerical simulation, the maximum compressive stress increment of the left structure is 0.71 MPa and the maximum tensile stress increment of the right structure is 0.15 MPa. However, in the model test, the maximum compressive stress increment of the left structure is 0.052 MPa. According to the stress similarity ratio, the actual engineering compressive stress increment is 1.04 MPa. The maximum tensile stress increment of the right structure is 0.056 MPa. According to the stress similarity ratio, the actual engineering tensile stress increment is 1.12 MPa. It can be found that the compressive stress and the tensile stress increments of the test results are larger than the numerical simulation results. The biggest difference between the model test and numerical simulation is that in numerical simulation, the change of the bending moment of the mining structure is smaller than that of each measuring point in the model test. On one hand, the strain gauges used in the model test are susceptible to test conditions and are prone to data fluctuations. On the other hand, in the model test, the change of the bending moment of the right wall is greater than that of

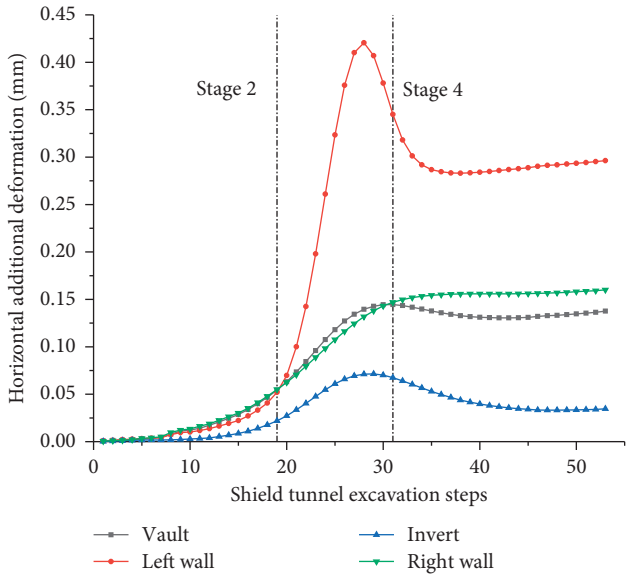

Figure 24: Support structure of the horizontal additional displacement curve.

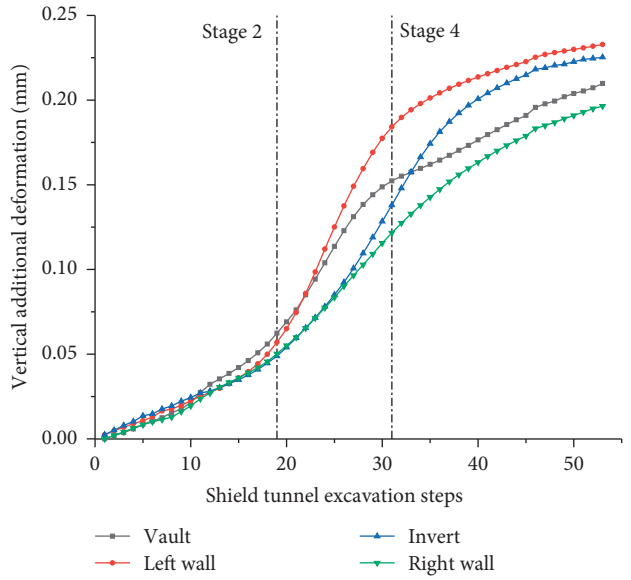

Figure 25: Support structure of the vertical additional displacement curve.

Table 8: Additional deformation of the right-line mining tunnel structure induced by left-line shield tunnelling.

Measuring point	Horizontal direction (mm)	Vertical direction (mm)	Ratio of vertical displacement (%)
Vault	0.13	0.21	61.7
Left waist	−0.09	0.23	71.8
Left wall	0.29	0.23	44.2
Left corner	−0.05	0.21	80.7
Invert	0.03	0.22	88.0
Right corner	0.04	0.19	82.6
Right wall	0.16	0.20	55.6
Right waist	−0.06	0.17	73.9

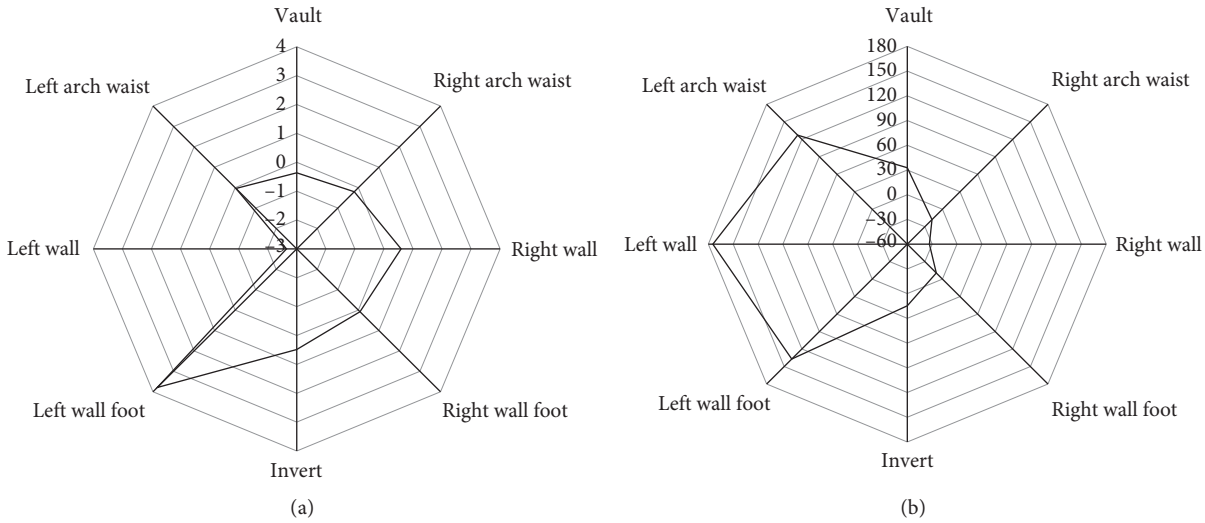

Figure 26: Additional internal force of the mining tunnel structure caused by shield tunnel. (a) Additional bending moment of the right-line mining tunnel affected by shield tunnel (unit: kN·m); (b) additional axis force of Right-line mining tunnel affected by shield tunnel (unit: kN).

the left side. Considering the difference of the soil disturbance induced by the shield tunnelling, the numerical calculation is more accurate and reasonable.

Comparing with the existing reference [26], the shield construction machinery used in this paper is relatively simple in use and low in cost. The process of this test simulated the important construction process of shield tunnelling, cutting soil, excavation, and assembling tunnel lining. However, the shield tunnelling machine used in the test did not simulate the complicated process of synchronous grouting, which is the shortcoming of this paper.

5. Study on the Influence Zone

In Sections 3 and 4, the influence of shield tunnelling on the mining tunnel under specific burial depth and clear distance has been discussed. However, the influence of different burial depth and tunnel clear distance is unknown. Therefore, considering the influence of tunnel clear distance and buried depth, the influence zone is proposed.

5.1. Determination of Discrimination Threshold. The determination of judgment criteria and related thresholds directly affects the delimitation of adjacent partitions. Common adjacent impact criteria are mainly divided into three categories: stratigraphic criteria, existing structural criteria, and composite criteria [37]. There are a large number of buildings above the metro tunnel. It is necessary to ensure that the ground settlement induced by the construction of two parallel tunnels does not affect the safety of the ground buildings. Therefore, the ground settlement induced by shield tunnelling and mining tunnelling construction is taken as the index to determine the adjacent influence zone [11].

The Chinese code for monitoring measurement of urban rail transit engineering [38] has corresponding provisions for the final settlement of the shield tunnel and mining tunnel construction. The determination threshold of ground settlement is shown in Table 9.

5.2. Numerical Models. In order to obtain the influence of shield tunnelling on the existing mining tunnel, 16 kinds of simulated conditions were established with considering the different clear distance and burial depth of the two tunnels, as shown in Table 10 and Figure 27. The mining tunnel is much larger than the shield tunnel. Therefore, the diameter of 6.28 m of shield tunnelling was used as the standard unit D to measure the relative position of the two tunnels. The determination of the buried depth of the tunnels is based on the mining tunnel. The dimensions of the calculation models for each condition are consistent, with 150 m in length, 70 m in width, and 88 m in height. As for the boundary conditions of the model, the displacement of the normal direction of each face of the model is constrained except the top surface. The numerical simulations and calculation parameters are consistent with those in Section 4.

5.3. Influence Zoning. The variation of surface subsidence under 16 working conditions was obtained, as shown in Table 11. As Table 11 illustrates, the final surface settlement decreased with the increase of burial depth and clear distance. Based on the criterion of surface subsidence, the key points of the boundary were calculated by interpolation and the influence zone is obtained, as shown in Figure 28.

Under actual conditions, the depth of the mining tunnel is about 3.46D and the horizontal clear distance is about 0.74D, which belongs to the weak influence zone. According to the conclusion of Section 4.4.1, the increment of ground settlement induced by shield tunnelling accounts for 3.9% of

Table 9: Ground settlement criterion discriminant threshold.

Influence zone	Surface subsidence (mm)
Effectless zone	<10
Weak influence zone	10–30
Strong influence zone	>30

Table 10: Numerical simulation conditions and numbers.

Clear distance	Buried depth			
	1.0D	2.0D	4.0D	6.0D
0.5D	1	2	3	4
1.0D	5	6	7	8
1.5D	9	10	11	12
2.0D	13	14	15	16

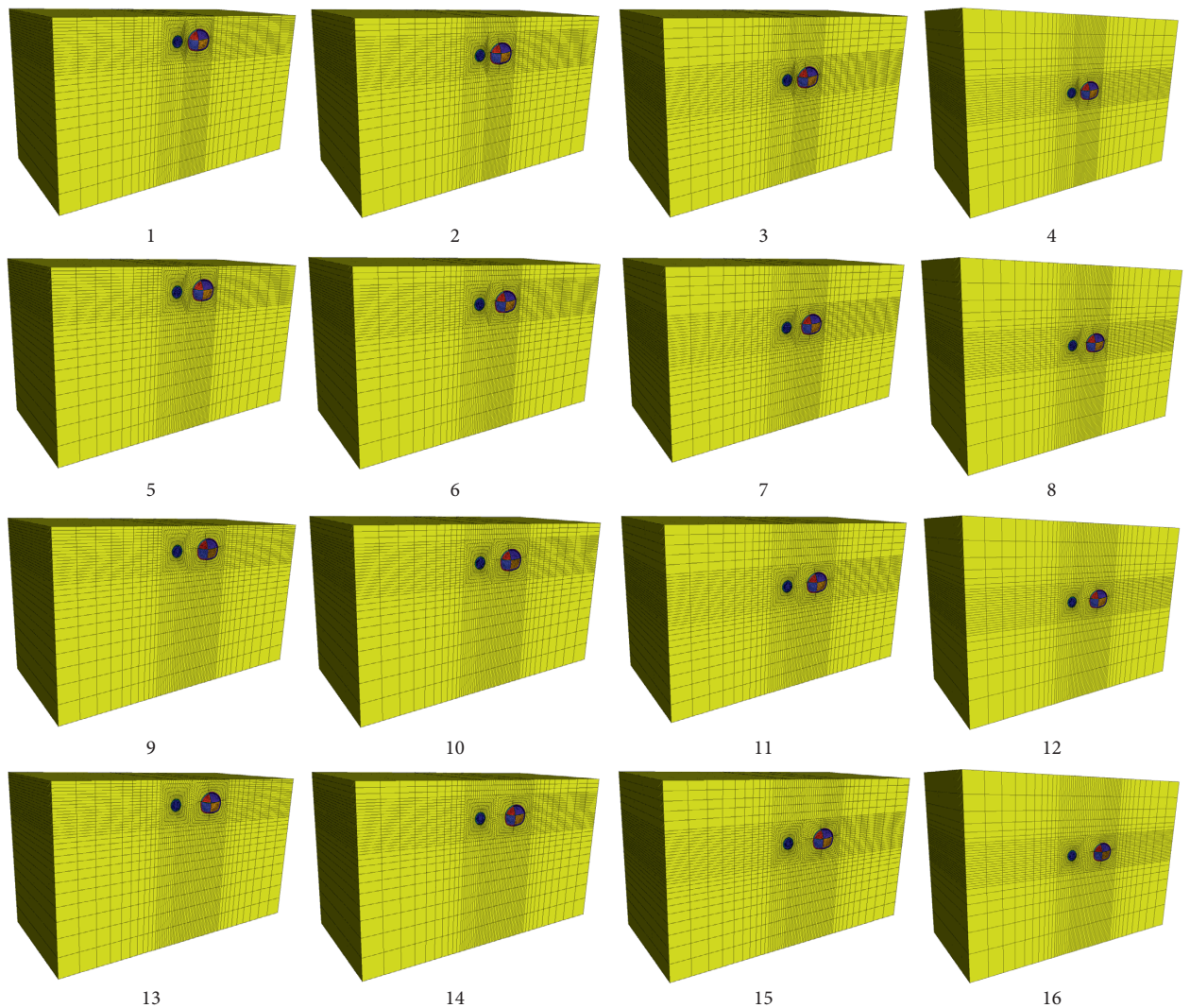

Figure 27: Numerical calculation model of 16 conditions.

Table 11: Maximum settlement on the surface of each working condition (unit: mm).

Clear distance	Buried depth			
	1.0D	2.0D	4.0D	6.0D
0.5D	−35.8	−32.7	−16.7	−5.1
1.0D	−33.9	−30.1	−14.4	−4.9
1.5D	−32.3	−28.5	−12.7	−4.7
2.0D	−31.7	−27.7	−11.5	−4.9

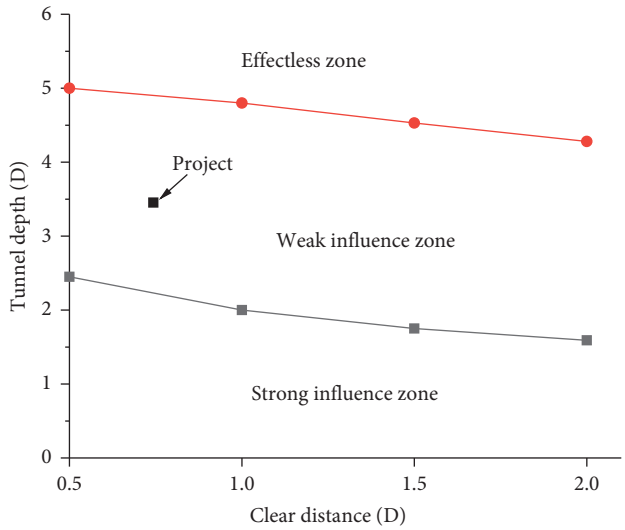

Figure 28: Surface subsidence criteria affect partition.

the maximum settlement. Meanwhile, according to the results of Section 3.4.3, the maximum settlement increment induced by shield tunnelling is 1 mm. Therefore, the final settlement after conversion is 25.6 mm, so the project is in the weak influence area of construction. It can be considered that the model test proves the rationality of the influence zone in this paper.

6. Conclusions

This paper is based on the shield tunnelling adjacent to the mining tunnel in Changsha Rail Transit Line 3. By carrying out the model test and numerical simulations, the following conclusions are obtained:

(1) Shield tunnelling has great difference in disturbance of surrounding rock around the existing mining tunnel. The closer to the new tunnel, the more obvious the surrounding rock stress changes. The influence of the internal force is performed as the asymmetric change of the internal force of the mining tunnel. The closer to the shield tunnel, the more severe the internal force of the structure changes. The structure near the shield tunnel is strengthened by pressure, and the structure far away from the shield tunnel is more prone to tensile failure.

(2) Shield method can effectively control surface settlement compared with the mining method. The shield machine tunnels forward from one time the excavation diameter before the monitoring section until the monitoring section completes the segment assembly. This process is the main stage that causes the increase in the corresponding surface settlement and the additional displacement of the existing mining tunnel. The influence on the mining tunnel structure is mainly vertical additional deformation, which is manifested as the overall floating of the mining tunnel.

(3) For argillaceous siltstone formation, considering the influence of tunnel clear distance and buried depth, the influence zone is proposed based on the criterion of surface subsidence. The rationality of the influence zone is verified by the numerical simulation and model test. The research results can provide reference for similar projects of the Changsha metro.

Data Availability

The data used to support the findings of this study are available from the corresponding author upon request.

Conflicts of Interest

The authors declare no conflicts of interest.

Acknowledgments

This work was supported by the Key Projects of Science and Technology Development Plan of China Railway Co., Ltd (grant no. 2017-14).

References

[1] R. P. Chen, J. Zhu, W. Liu, and X. W. Tang, "Ground movement induced by parallel EPB tunnels in silty soils," *Tunnelling and Underground Space Technology*, vol. 26, no. 1, pp. 163–171, 2011.

[2] F.-y. Meng, R.-p. Chen, and X. Kang, "Effects of tunneling-induced soil disturbance on the post-construction settlement in structured soft soils," *Tunnelling and Underground Space Technology*, vol. 80, pp. 53–63, 2018.

[3] Z. Xufeng, W. Chunmiao, S. U. N. Jinglin, and K. Xiangli, "Analysis of mechanical action of shield driving for approaching excavation," *Rock and Soil Mechanics*, vol. 28, pp. 409–414, 2007.

[4] J.-I. Choi and S.-W. Lee, "Influence of existing tunnel on mechanical behavior of new tunnel," *KSCE Journal of Civil Engineering*, vol. 14, no. 5, pp. 773–783, 2010.

[5] D.-M. Zhang, Z.-K. Huang, Z.-L. Li, X. Zong, and D.-M. Zhang, "Analytical solution for the response of an existing tunnel to a new tunnel excavation underneath," *Computers and Geotechnics*, vol. 108, pp. 197–211, 2019.

[6] H. Chakeri, R. Hasanpour, M. A. Hindistan, and B. Ünver, "Analysis of interaction between tunnels in soft ground by 3D numerical modeling," *Bulletin of Engineering Geology and the Environment*, vol. 70, no. 3, pp. 439–448, 2011.

[7] Z. Zhang, M. Huang, C. Zhang, K. Jiang, and M. Lu, "Time-domain analyses for pile deformation induced by adjacent excavation considering influences of viscoelastic mechanism," *Tunnelling and Underground Space Technology*, vol. 85, pp. 392–405, 2019.

[8] Z. Zhang, C. Zhang, K. Jiang et al., "Analytical prediction for tunnel-soil-pile interaction mechanics based on Kerr foundation model," *KSCE Journal of Civil Engineering*, vol. 23, no. 6, pp. 2756–2771, 2019.

[9] Z. Zhang, M. Huang, C. Xu, Y. Jiang, and W. Wang, "Simplified solution for tunnel-soil-pile interaction in Pasternak's foundation model," *Tunnelling and Underground Space Technology*, vol. 78, pp. 146–158, 2018.

[10] Z. Zhang, M. Huang, X. Xi, and X. Yang, "Complex variable solutions for soil and liner deformation due to tunneling in clays," *International Journal of Geomechanics*, vol. 18, no. 7, Article ID 04018074, 2018.

[11] R. Chen, F. Meng, Z. Li, Y. Ye, and J. Ye, "Investigation of response of metro tunnels due to adjacent large excavation and protective measures in soft soils," *Tunnelling and Underground Space Technology*, vol. 58, pp. 224–235, 2016.

[12] R. Pan, Q. Wang, B. Jiang, and S. Li, "Model test on failure and control mechanism of surrounding rocks in tunnels with super large sections," *Arabian Journal of Geosciences*, vol. 12, no. 22, p. 17, 2019.

[13] T. Lianjin, S. Bin, and L. Xiaolin, "Interaction analysis of double holes extremely close approaching parallel shield tunnels construction," *Chinese Journal of Rock Mechanics and Engineering*, vol. 28, pp. 1856–1862, 2009.

[14] X. Kong, C. Xia, Y. Qiu, L. Zhang, and J. Gong, "Study of construction mechanical behavior of parallel-small spacing metro tunnels excavated by shield method and cross diaphragm (CRD) method in loess region," *Rock and Soil Mechanics*, vol. 32, pp. 516–524, 2011.

[15] L. Daiguo, Z. Changqun, T. Xia, D. Shaolin, and C. Jianping, "Mechanical effects of adjacent metro shield construction of the first hole on the second hole," *Journal of Central South University (Science and Technology)*, vol. 48, pp. 1027–1034, 2017.

[16] X.-T. Lin, R.-P. Chen, H.-N. Wu, and H.-Z. Cheng, "Deformation behaviors of existing tunnels caused by shield tunneling undercrossing with oblique angle," *Tunnelling and Underground Space Technology*, vol. 89, pp. 78–90, 2019.

[17] D. Jin, D. Yuan, X. Li, and H. Zheng, "Analysis of the settlement of an existing tunnel induced by shield tunneling underneath," *Tunnelling and Underground Space Technology*, vol. 81, pp. 209–220, 2018.

[18] W. Qian, T. Qi, Y. Zhao, Y. Le, and H. Yi, "Deformation characteristics and safety assessment of a high-speed railway induced by undercutting metro tunnel excavation," *Journal of Rock Mechanics and Geotechnical Engineering*, vol. 11, no. 1, pp. 88–98, 2019.

[19] W. Ming-nian, Z. Xiao-jun, G. Ming-zhong, and C. Guang-yao, "Method of three-dimensional simulation for shield tunneling process and study of adjacent partition of overlapped segment," *Rock and Soil Mechanics*, vol. 33, pp. 273–279, 2012.

[20] Z. Ding, Y. Wu, X. Zhang, and K. Chen, "Numerical analysis of influence of shield tunnel in soft soil passing over existing nearby subway," *Journal of Central South University (Science and Technology)*, vol. 49, pp. 663–671, 2018.

[21] W. Zhao, P.-j. Jia, L. Zhu et al., "Analysis of the additional stress and ground settlement Induced by the construction of double-o-tube shield tunnels in sandy soils," *Applied Sciences*, vol. 9, no. 7, p. 1399, 2019.

[22] X.-T. Lin, R.-P. Chen, H.-N. Wu, and H.-Z. Cheng, "Three-dimensional stress-transfer mechanism and soil arching evolution induced by shield tunneling in sandy ground," *Tunnelling and Underground Space Technology*, vol. 93, Article ID 103104, 2019.

[23] H. Cheng, J. Chen, and G. Chen, "Analysis of ground surface settlement induced by a large EPB shield tunnelling: a case study in Beijing, China," *Environmental Earth Sciences*, vol. 78, no. 20, 2019.

[24] V. Fargnoli, D. Boldini, and A. Amorosi, "TBM tunnelling-induced settlements in coarse-grained soils: the case of the new Milan underground line 5," *Tunnelling and Underground Space Technology*, vol. 38, pp. 336–347, 2013.

[25] X. Tan, H. Zhang, G. Zhang, Y. Zhu, and P. Tu, "An improved method for predicting the greenfield stratum movements caused by shield tunnel construction," *Applied Sciences*, vol. 9, no. 21, p. 4522, 2019.

[26] W. Ding, C. Duan, Y. Zhu, T. Zhao, D. Huang, and P. Li, "The behavior of synchronous grouting in a quasi-rectangular shield tunnel based on a large visualized model test," *Tunnelling and Underground Space Technology*, vol. 83, pp. 409–424, 2019.

[27] Y. Fang, Z. Chen, L. Tao, J. Cui, and Q. Yan, "Model tests on longitudinal surface settlement caused by shield tunnelling in sandy soil," *Sustainable Cities and Society*, vol. 47, p. 101504, 2019.

[28] G. Zheng, Y. Lei, T. Cui et al., "Experimental research on the transverse effective bending rigidity of shield tunnels," *Advances in Civil Engineering*, vol. 2019, Article ID 2174562, 17 pages, 2019.

[29] Q. Gong, Y. Zhao, J. Zhou, and S. Zhou, "Uplift resistance and progressive failure mechanisms of metro shield tunnel in soft clay," *Tunnelling and Underground Space Technology*, vol. 82, pp. 222–234, 2018.

[30] S.-L. Shen, H.-N. Wu, Y.-J. Cui, and Z.-Y. Yin, "Long-term settlement behaviour of metro tunnels in the soft deposits of Shanghai," *Tunnelling and Underground Space Technology*, vol. 40, pp. 309–323, 2014.

[31] D. Jin, D. Yuan, S. Liu, X. Li, and W. Luo, "Performance of existing subway tunnels undercrossed by four closely spaced shield tunnels," *Journal of Performance of Constructed Facilities*, vol. 33, no. 1, Article ID 04018099, 2019.

[32] J.-r. Zhang, K.-g. Sun, F. Lu, Z.-x. Zheng, and Q.-q. Sun, "Model test study of surrounding rock pressure distribution and mechanical characteristics of unequal-span double-arch railway tunnel," *Rock and Soil Mechanics*, vol. 36, p. 3077, 2015.

[33] C. Liu, S. Li, Z. Zhou, L. Li, K. Wang, and C. Qin, "Model test study on spatial deformation law of surrounding rock for super-large section and shallow buried tunnels," *Geotechnical Testing Journal*, vol. 42, no. 3, Article ID 20170243, 2019.

[34] R. Shah, A. Lavasan, D. Peila, C. Todaro, A. Luciani, and T. Schanz, "Numerical study on backfilling the tail void using a two-component grout," *Journal of Materials in Civil Engineering*, vol. 30, no. 3, Article ID 04018003, 2018.

[35] J. Zou and S. Zuo, "Similarity solution for the synchronous grouting of shield tunnel under the vertical non-axisymmetric displacement boundary condition," *Advances in Applied Mathematics and Mechanics*, vol. 9, no. 1, pp. 205–232, 2017.

[36] X. Xie and G. Tang, "Effects of curved shield tunnelling adjacent to existing power tunnel," *European Journal of*

Environmental and Civil Engineering, vol. 22, no. sup1, pp. s164–s178, 2018.

[37] W. Qiu, *The Study on Mechanics Principle and Countermeasure of Approaching Excavation in Underground Works*, Southwest Jiaotong University, Chengdu, China, 2003.

[38] China Architecture and Building Press, *Code for Monitoring Measurement of Urban Rail Transit Engineering*, China Architecture and Building Press, Beijing, China, 2014.